Measurement of particle dynamics in rapid granular shear flows

Zafar Mahmood[1], Subodh Dhakal[2], Kazuyoshi Iwashita[3]

ABSTRACT: Micromechanics of rapid granular flows is studied in a two-dimensional planar granular Couette flow apparatus. The device is capable of generating particulate flows at different shearing rates and solid fractions. Mono size plastic disks are sheared across an annular test-section for several shear rates. Motion of particles is recorded through high speed digital camera and analyzed by image processing techniques. The average and fluctuation velocity profiles are obtained and granular temperature relations with shear rate are investigated. Average streaming velocity across the shear cell decays slightly faster than exponential, and is rather Gaussian when not too close to the wall. Fluctuation velocities and granular temperature across the shear cell are related to effective shear rate. Interparticle collisions are estimated from the particle trajectories and probability distribution of collision angles obtained from particle collision data. In dense flows, three peaks of collision angles are observed which signal the onset of triangular structure formulation and cause crystallization. It is found that the distribution of collision angles is anisotropic.

CE Database subject headings: Couette flows; Flow properties; Granular temperature; Interparticle collisions

---

[1] PhD student, Saitama University, Department of Civil and Environmental Engineering, 255 Shimo-Okubo, Sakura-ku, Saitama 338-8570, Japan. Tel. No. +81-48-858-3545, Fax No. +81-48-858-7374, E-mail: zafar7374@yahoo.com (corresponding author)

[2] PhD student, Saitama University, Department of Civil and Environmental Engineering, 255 Shimo-Okubo, Sakura-ku, Saitama 338-8570, Japan. E-mail: 05d2057@mail.saitama-u.ac.jp

[3] Professor, Saitama University, Department of Civil and Environmental Engineering, 255 Shimo-Okubo, Sakura-ku, Saitama 338-8570, Japan. E-mail: iwa@mail.saitama-u.ac.jp

Introduction

Flowing granular materials are commonplace in numerous terrestrial processes. A granular material is a collection of a large number of discrete solid particles, e.g. landslides, sediment transport, and pneumatic transport of particulate solids in various manufacturing systems. In these granular material flows, the random motions of particles resulted from the interactive collisions of particles is the dominant mechanism affecting the flow behavior (Campbell 1990). Because of the random motions of particles in a granular flow which are similar to the motions of molecules of gas, the concepts in the dense-gas kinetic theory (Savage and Jeffrey 1981; Jenkins and Savage 1983; Lun et al. 1984; Jenkins and Richman 1985) are borrowed to model and analyze the granular flow behavior.

The term granular temperature is defined as the specific fluctuation kinetic energy of particles to quantify the random motions of particles (Ogawa 1978). It is assumed that the collisions are binary and isotropic in the granular flows. Thus the assumption of isotropic granular temperature distribution is also applied, despite the fact that this key assumption might not be applicable in most of particle granular material flow systems (Campbell 1990).

Experimental studies on granular flows are rather scarce and generally restricted to bulk flow measurements. There is some data on the details of the flow properties such as mean velocity profiles, fluctuation velocity components and granular temperature. More importantly, there is practically no experimental data on the interparticle collisions during rapid flows of granular materials. Earlier experimental studies generally restricted to bulk flow measurements. Savage and Sayed (1984) and Hanes and Inman (1985) reported variation of bulk shear and normal stresses with shear rate and solid volume fraction.

In the last decade, the image technology has been widely used to measure the two-dimensional fluctuations and granular temperature in inclined chutes (Drake 1991), in vertical channels (Natarajan et al. 1995), in vibrated beds (Warr et al. 1994; Hsiau et al. 2002) and shear cells (Elliot et al. 1998; Hsiau and Jang 1998; Hsiau and Shieh 1999). Most studies show that the granular temperature distributions are anisotropic.

Because of its simplicity, the granular Couette flow is very suitable for fundamental research (Savage and Sayed 1984; Hanes and Inman 1985; Johnson and Jackson 1987; Wang and Cambpell 1992; Hsiau and Jang 1998; Hsiau and Yang 2005). This paper describes a series of tests to measure flow properties (velocity profiles, velocity fluctuations, and granular temperature) and interparticle collisions of two-dimensional sheared granular flows generated in a rotated Couette shear cell. Since the particles are forced to move in a horizontal plane, their

trajectories could be followed easily by a high speed digital camera. A digital image processing procedure is then used to measure the instantaneous velocities for various solid volume fractions and shearing rates. Using an averaging technique, experimental data for variations of granular mean velocity, root mean square (RMS) fluctuating velocities, and granular temperature across the shearing cell are obtained. Collisions are estimated from the particle trajectories and collision angle distributions are studied.

Experimental Apparatus and Procedure

Experimental apparatus

In this section, the experimental setup used in the study including the shear cell device and the image processing system is described. Moreover, calculation of average, fluctuation velocities, granular temperature and particle collision algorithm based on particle trajectories is also described.

A mono-granular shear flow apparatus used for the studies is the same, with only minor modifications, as that used by Iwashita et al. (2004). Fig. 1 shows the plan view and cross section of the apparatus respectively. Table 1 shows the capacity of apparatus. The particles used in the experiment are plastic disks of diameter d =2.3 cm, a density of 0.934 g/cm^3. To measure the particle movement more precisely with particle tracking method, disks with mark at their centers are used instead of spheres. Table 2 shows the properties of particles used in experiment. The apparatus consists of an inner and outer cylindrical walls resting on a bottom horizontal plate (radii 28.5 & 40 *cm* respectively). The upper plate consists of arcylic. The inner wall moves to generate the shear flow. The spacing between the inner and outer walls, called shear cell height, is H=11.5 *cm* which is equivalent to five particle diameters, while the distance between the upper and lower plates is only 8 *mm* which is somewhat larger than the particle thickness. If shear cell height is increased, most of shearing would occur near the moving wall leaving rest of region in crystallized state. Rotation speed of inner wall can be changed freely. The outer wall is placed on horizontal steel plate through several ball bearings to minimize the friction between them. Since particles move on horizontal plane, gravity may take any small effect on the movement of granular particles.

In order to satisfy the condition that shear cell be a part of granular flow, inner wall is roughened by means of gluing circular flanges of same radius as the plastic disks. The shear rate, $\dot{\gamma} = V_w / H$ (defined as ratio of inner

wall velocity, V_w and shear cell height H), is freely controlled by means of velocity, V_w , of inner wall. In this study, shear rate was varied from 10.6 to 37.1 sec^{-1}.

A high speed video camera (FASTCAM-X 1280 PCI, frame rate in this experiment: 1,000 frames per second) connected with a frame grabber was used to record the flow. Table 3 shows the capacity of video camera. Particles were tracked using a particle tracking software "Dipp-Motion XD". Coordinates of center of each particle were mapped at each frame and used to evaluate the instantaneous position of the granules.

The mean normalized fraction was initially estimated as a function of the maximum packing factor (MPF) allowed by the geometry of the setup. Here, the MPF is defined as the ratio of the area of the maximum number of particles which can occupy a specific area, to the total area. For an unbounded region, the maximum packing factor for disks is 0.907 (Elliot et al. 1998). For the experimental shear cell configuration (the annulus between the inner and the outer cylinders) the maximum packing factor was 0.795. Using the estimated valued for the MPF, the number of particles required for bulk surface fraction (or normalized fraction) of roughly 60% to 80% were used in the shearing cell. The details of shear rate and solid fractions used during the experiment are shown in Table 4.

Experimental procedure

In this section the procedure for the experimental study is outlined and the method for analyzing images is discussed. The averaging techniques for velocity are also described.

The camera was set up vertically and was focused onto the test section of the shearing cell. The size of the test section was 20 x 11.5 cm. A shutter speed of 1/1,000 sec was used to ensure an accurate image of each particle. Each experimental run consisted of 2,000 digital video frames of resolution 1,280 x 512 pixels and imaging about 200 to 400 particles depending upon the concentration. The positions of the center of each disk were recorded. The coordinates (x_{1j} , y_{1j}) of jth particle from frame 1 were recorded, and mapped to frame 2 where their new coordinates were recorded as (x_{2j} , y_{2j}) and so on. The friction between the apparatus floor and disks was not accounted for which may influence the particle movement and generated stress in the flow.

The particles in the recorded digital video frames were tracked by a particle tracking software "Dipp-Motion XD". The center of disk was marked and tracked through the software. The positions were recorded in pixels, and then converted into physical coordinates. (For the condition of the experiment, there were 18 pixels per cm.)

The velocities of individual particles and the concentration profile of the flow were then evaluated from the locations of the disk centers on successive frames. The test section of the shearing cell is broken into 9 overlapping bins of width "*d*" as shown in Fig. 2.

Particle velocities (V_θ, V_r) described in relation to the Cartesian (x_j, y_j) coordinate system were evaluated. V_θ is the streaming component and V_r is the transverse component respectively. The instantaneous velocity of the "*jth*" particle in the streaming direction was estimated as

$$u_j = \frac{(x_{2j} - x_{1j})}{0.001\,sec}, \qquad (1)$$

where x_{1j} and x_{2j} are the respective x coordinates of particle "*j*" mapped from frame 1 to 2, and 0.001 *sec* is the time difference of exposure between successive frames. The averages velocities in streaming direction were then computed for each bin (i = 1,2,3…,9) across the test-section according to

$$V_\theta^{(i)} = \frac{1}{N_{pi}} \sum_{j=1}^{N_{pi}} u_j^{(i)}, \qquad (2)$$

where N_{pi} is the number of velocities used for averaging the mean values. The transverse instantaneous velocity v_j and the average $V_r^{(i)}$ for each bin were computed in exactly the same manner using y_{1j} and y_{2j} as the respective particle coordinates.

Once the average $V_\theta^{(i)}$ and $V_r^{(i)}$ velocities were determined for each bin, their respective root-mean-square (RMS) fluctuating velocities were estimated by

$$v'^{(i)}_\theta = \sqrt{\frac{1}{N_{pi}} \sum_{j=1}^{N_{pi}} \left(u_j^{(i)} - V_\theta^{(i)}\right)^2} \quad \text{and} \quad v'^{(i)}_r = \sqrt{\frac{1}{N_{pi}} \sum_{j=1}^{N_{pi}} \left(v_j^{(i)} - V_r^{(i)}\right)^2}, \qquad (3)$$

The granular temperature *T*, also called averaged fluctuation kinetic energy, for each bin was calculated using the expression

$$T^{(i)} = \frac{1}{2}\left(v'^{(i)2}_\theta + v'^{(i)2}_r\right). \qquad (4)$$

The shearing cell was divided into three bins each of width twice the diameter of disk, and overlapping half the diameter. Velocity distribution in the streaming and transverse direction was determined in each bin. The velocity was divided into regions of width ΔV =10 cm/s. The velocity of particles falling in each region was counted.

The totals in each region were normalized by dividing by the total number of velocity counts and by the region width.

The two-dimensional average solid fraction, ν, and normalized solid fraction, ν^*, was determined for each experimental flow condition as

$$\nu = \frac{\left(0.25\pi d^2\right)\left(N_{cell}\right)}{A_{cell}}, \quad \nu^* = \frac{\nu}{\nu_m} \tag{5}$$

where A_{cell} is the shearing cell area and N_{cell} represents the total number of particles introduced into the shearing cell for a specific flow, and ν_m is the maximum packing for disks in two-dimension for the experimental setup (the value for experiment is 0.795).

The collision events have been identified from the trajectories by using the following algorithm. All velocity vectors $\vec{V}$ were compared sequentially to find direction changes given by

$$\psi = \cos^{-1}\left(\hat{V}_i \cdot \hat{V}_j\right), \tag{6}$$

where $\hat{V} = \vec{V}/\left|\vec{V}\right|$ is the unit vector of the calculated velocity, and subscripts *i*, *j* represent positions separated by the time difference $\Delta t = 0.001$ sec.

The collision algorithm consists of following two conditions:

Condition 1: If $30^\circ \le \psi \le 180^\circ$, the proximity of all particles at the same time instant were checked. If a particle were found within a radius $d + \Delta d$, whose velocity also satisfied Eq. 6, it was considered as a candidate for a collision ($\Delta d = 0.1d$). To assure that recollision were not occurring; a record of the identity of the previous collision partner was maintained. It was then ensured that those particles can recollide if and only if the partner particle has undergone a collision with yet a third particle. The collision was considered if particle satisfied all the above requirements. In this study, collisions of particles with boundary walls were not measured.

Condition 2: If condition 1 was not satisfied, condition 2 was considered. The velocity change was determined using

$$\Delta V = \frac{\left|V_i - V_j\right|}{V_{\min}} \times 100, \tag{7}$$

where ΔV is the percent velocity difference of a particle between two positions i and j, and $V_{\min}$ is the minimum of V_i and V_j. If $\Delta V \geq 200$ the proximity of all particles at the same time instant were checked. If a particle were found with in a radius $d + \Delta d$ which also satisfied Eq. 7, it was considered as a candidate for a collision. The rest of method is same as described in condition 1. The collision algorithm is described in Fig. 3.

There is an angle θ that is characteristic of each collision between two particles (measured in counterclockwise direction and defined as shown in Fig. 3 and 12). The range of θ is $0 \leq \theta \leq 360^\circ$. The datum, θ=0, is arbitrary. The collision distribution was measured in much the same way as the velocity distribution. The region $0 \leq \theta \leq 360^\circ$ was divided into 120 regions. The number of collisions that occurred in each region was counted. The totals in each region were normalized by dividing by the total number of collisions and by the region width. The shearing cell was divided into three bins each of width twice the diameter of disk, and overlapping half the diameter. The collision angle distribution was determined for each bin.

The spatial arrangement and principal direction of collision angles was determined using fabric tensors (Oda and Iwashita 1999).

Experimental Results and Discussions

The experimental data for a range of normalized fractions and shear rates are compiled and some sample results are described.

Average velocity profiles

Fig. 4 shows the experimental data for the mean velocity in streaming direction for normalized fraction of 0.70 for different shear rates in the shear cell. The streaming velocity is normalized by inner wall velocity while the distance, *r*, measured from the inner moving wall is non-dimensionalized by dividing with particle diameter *d*. It is clear from Fig. 4a that in rapid shearing regime, the velocity profile normalized by inner wall velocity is invariant to the imposed shear rate at the inner wall. Further, the velocity decays quickly across the shear cell as the distance *r* increases, i.e. the shearing is localized near the moving wall. Fig. 4b shows that velocity decays slightly faster than exponential. Also the logarithmic plot of the velocity profile versus $(r/d)^2$ (Fig. 4c) shows that the velocity profile is

rather Gaussian when not too close to the wall. The solid line in Fig. 4c is the fitting curve to the experimental data. All flow exhibited across the shear cell can be expressed through equation $V_\theta(r) = aV_w \exp\left[-b(r/d)^2\right]$ where a, b are the fitting parameters, r is distance from moving wall, V_w is the velocity of moving wall, V_θ is the average velocity of disks in the steaming direction, and d is disk diameter. For the current experiment, values of parameter a ranges from 0.42 to 0.80 and parameter b ranges from 0.17 to 0.27 for normalized fraction of 0.60 to 0.80 respectively. Both exponential and Gaussian fits have been proposed for the velocity profiles (Veje et al. 1999; Bocquet et al. 2002; Mueth 2003). The velocity profiles in the present study are qualitatively similar to those reported by MIDI (2004) and Mueth (2003). Although a fitting form of $V_\theta(r)$ was not given for the MIDI (2004) data, inspection of Figs. 3d and 3e in MIDI (2004) reveals that the overall shape of $V_\theta(r)$ exhibits curvature (on a log-linear plot) similar to what we observe in Figs. 4b and 4c respectively. The velocity profile is smooth and does not show the strong steps seen with MRI experiments, as video techniques track the particle center motion and not the average flow of material, as MRI does. From Fig. 4, it is clear that there exits a slip at the inner moving wall. Parameter a reflects the slip at the inner moving wall. Slip velocity is defined as the difference between the wall velocity and the average particle velocity in the bin adjacent to the inner wall. Fig. 5a shows variations of slip velocity with particle concentration for shear rates ranging from 17.8 $sec^{-1} \le \dot{\gamma} \le 20.2$ sec^{-1} to 32.3 $sec^{-1} \le \dot{\gamma} \le 34.7$ sec^{-1}. The slip velocity is normalized with inner wall velocity. It is observed that the slip velocity decreases as the normalized fraction increases. Fig. 5b shows the variation of normalized slip velocity with shear rate for particle concentrations of 0.60 to 0.80. It is observed that for a fixed particle concentration, the slip velocity normalized with inner wall velocity remains same with shear rate.

Probability distribution of particles velocities

The velocity components in the streaming direction, v_θ, and transverse direction, v_r were histogrammed for all particles and times for several ranges of radii r (Fig. 6). These velocities represent the measured average velocity between two successive frames (i.e. over 0.001 *sec*). The investigation area was divided into three overlapping bins. Each curve in Fig. 6 represents particles at different radii: $0<r/d<2$ (squares), $1.5<r/d<3.5$ (circles), and $3<r/d<5$ (triangles). The average velocity in the streaming direction is plotted as small vertical line at the top of Fig. 6a labeled by the symbol of the curve which it corresponds to. The velocity distributions $P(v_\theta)$ are peaked near their

average value. Fluctuations away from the mean velocity decay roughly exponentially, especially far from the inner moving wall, but acquire a rounded shape for small *r*. The width of the distributions decreases with increasing distance *r* from the moving wall. The width of curve is reflected by the RMS fluctuating velocity, i.e., higher the fluctuating velocity, the wider the curve. The most probable streaming velocity in the region 3<r/d<5 (i.e. near the outer wall) is zero, which indicates crystallization. Transverse velocity distribution $P(v_r)$ is peaked at $v_r = 0$ as shown in Fig. 6b and is approximately symmetric about this point, since the primary flow is not in the transverse direction.

Velocity fluctuations profiles

The root-mean square (RMS) fluctuation velocity profiles were studied for different normalized fractions. (e.g. Fig. 7 shows the fluctuation velocity profiles for $\nu^* = 0.60$). In order to relate the velocity fluctuations with shear rate (or inner wall velocity), $\nu'^2/\left(V_w\sqrt{gd}\right)$ and $T/\left(V_w\sqrt{gd}\right)$ are plotted as a function of r/d. The purpose of using *g* here is only to non-dimensionalize the fluctuation velocity components and shear rate. As shown in Fig. 7, the velocity fluctuations decrease exponentially with distance to the moving wall. Further, it is evident that non-dimensional fluctuation velocity profile, $\nu'^2/\left(V_w\sqrt{gd}\right)$, and granular temperature profile, $T/\left(V_w\sqrt{gd}\right)$ are roughly independent of shear rate. The typical velocity fluctuations ν'^2 do not scale with V_w^2 but rather with wall velocity V_w as shown in the Fig. 7. The velocity fluctuations in streaming direction are slightly higher than the transverse direction. The root-mean square fluctuation velocities in streaming direction, $v_\theta'^2$, and transverse direction, $v_r'^2$, decay more slowly with r than does the average velocity, $v_\theta(r)$.

Variation of fluctuation velocities and granular temperature with shear rate

The shearing experienced by the bulk of granular layer is less than the ideal shear rate due to slipping at the moving wall. The effective shear rate, $\dot{\gamma}_{eff} = V_\theta^{(1)}/H$, is the shearing experienced by the granular material, where $V_\theta^{(1)}$ is the average streaming velocity in bin 1 (i.e. bin next to inner moving wall). The relationship between the dimensionless fluctuation velocity components through the shear cell (i.e. $v_r'/\sqrt{gd}$, $v_\theta'/\sqrt{gd}$) and dimensionless effective shear rate, $\dot{\gamma}_{eff}\sqrt{d/g}$ is shown in Fig. 8. The relationship for both streaming and transverse directions is consistent with a

power-law: $v_r' \propto \left(\dot{\gamma}_{eff}\right)^{\alpha}$ with $\alpha = 0.84$ for streaming direction and $v_\theta' \propto \left(\dot{\gamma}_{eff}\right)^{\alpha}$ with $\alpha = 0.81$ for transverse direction respectively. Since the fluctuation strengths are nearly identical in streaming and transverse direction (as shown in Fig. 8), this can be expressed in terms of granular temperature $T \equiv m(v')^2$, obtaining $T \propto \left(\dot{\gamma}_{eff}\right)^{2\alpha}$. With the measured value of α, these results are consistent with $T \propto \left(\dot{\gamma}_{eff}\right)^{1.66}$ (as shown in Fig. 9 when dimensionless granular temperature across the shear cell is plotted against dimensionless effective shear rate). Granular kinetic theory for fast, dilute flows predicts that $\dot{\gamma} \propto v' \propto \sqrt{T}$ for steady flow (Haff 1986). This is little inconsistent with our observations. This inconsistency may be due to several assumptions of kinetic theory that do not hold for dense flows. The modified hydrodynamic model of Bocquet et al. (2002) predicts $v' \propto \dot{\gamma}^{\alpha}$, even though it makes no prediction for the value of α other than $\alpha < 1$.

The relationship between granular temperature and effective shear rate is analogous to the experimental shear stress dependence on shear rate raised to the power 1.5 to 2. Earlier experiments (Savage and Sayed 1984; Hanes and Inman 1985; Bagnold 1954) have shown quadratic dependence of shear rate on shearing stress. While revisiting the Bagnold's experiments (1954), Hunt et al. (2002) have found that the experimental shear stress measurements do not show a quadratic dependence on shear rate; instead, the shear stress depends on the shear rate raised to the 1.5 power.

Probability distribution of collision angles

Figs. 10 & 11 show the probability distribution of collision angles for medium and dense flows (i.e. for normalized fractions of 0.70 and 0.80 respectively) for different shear rates. For each shear rate, the collision angle distribution is measured at three different radii in the shear cell, i.e. near the moving wall ($0 < r/d < 2$), in the mid region ($1.5 < r/d < 3.5$) and near the outer wall ($3 < r/d < 5$). It is observed that probability distribution of collisions in each region is higher on the upstream-faces of the colliding particles, i.e. for $\theta \in [0, \pi/2]$ and $\theta \in [\pi, 3\pi/2]$ (i.e. the hatched-areas on the test particle in Fig. 12). This is a consequence of the imposed shear field which compresses the flow structure along the $\pi/4$-direction and stretches it along $3\pi/4$-direction as shown by the peaks in these directions. While the peaks at θ approaching zero (i.e. $\theta \in [-\pi/4, 0]$) correspond to head-on collisions between

particles in the same layer (Fig. 10). The principal collision angles determined through fabric tensor analyses (dark solid lines in the Fig. 10 and 11) are along the $\pi/4$ -direction in the first quadrant (i.e. $\theta \in [0, \pi/2]$).

In the dense flow case (Fig. 11), the peaks in three directions i.e. along $\pi/4$ -direction, $3\pi/4$ -direction, and $\pi/2$ -direction signal the onset of triangular structure formulation which may cause crystallization and jamming of flow. Crystallization is also evident from probability distribution of particle velocities (Fig. 6) for the dense flow case. The most probable velocity in streaming as well as transverse direction is zero in region $3<r/d<5$, which indicates crystallization. From the analysis of the videos of experiment captured using high-speed camera, it is evident that column-like force chains form along $\pi/4$ -direction (i.e. the major peak and principal collision angle) while the particles move along $3\pi/4$ -direction and $\pi/2$ -direction after collapse of the force chains (i.e. the other two peaks). Another noteworthy point is that probability distribution of the collisions on the downstream-faces of the colliding particles is less than upstream-faces; hence collision angle distributions may be approximated solely by its contributions from the first and third quadrants (i.e. $\theta \in [0, \pi/2]$ and $\theta \in [\pi, 3\pi/2]$ respectively). The results of collision angle distributions and peaks are qualitatively similar to those reported by Alam and Luding (2003) in their numerical simulation of dense sheared granular fluid.

Conclusions

This paper studied the flow properties of mono size granular material in a two-dimensional shear cell. The image processing technology and particle tracking method were employed to measure the average, fluctuation velocity profiles, granular temperature and interparticle collisions. Four different solid fractions (0.60, 0.70, 0.75 and 0.80) were tested.

The average velocity profile normalized by the shear rate (i.e. inner wall velocity) is invariant to the imposed shear rate at the inner wall. Further, the velocity decays quickly across the shear cell as the distance *r* increases, i.e. the shearing is localized near the moving wall. Further, velocity decays slightly faster than exponential and is rather Gaussian when not too close to the wall.

We measured power-law relationship between effective shear rate and fluctuation velocities: $v_r' \propto (\dot{\gamma}_{eff})^{\alpha}$ with $\alpha = 0.84$ for streaming direction; $v_\theta' \propto (\dot{\gamma}_{eff})^{\alpha}$ with $\alpha = 0.81$ for transverse direction respectively. This result

is little inconsistent with granular kinetic theory for fast, dilute flows which predicts α = 1.0 (Haff 1986). This inconsistency may be due to several assumptions of kinetic theory that do not hold for dense flows.

Interparticle collisions were estimated from the particle trajectories and probability distribution of collision angles obtained from particle collision data. It is observed that probability distribution of collisions across the shear cell is higher on the upstream-faces of the colliding particles. In dense flows, three peaks of collision angles are observed which clearly signal the onset of triangular structure formulation and cause crystallization. It is found that the distribution of collision angles is anisotropic.

Acknowledgements

This study was performed at the Department of Civil and Environmental Engineering, Saitama University, Saitama. The authors appreciate a great help of their colleagues in the experimental work. This research was partially supported by Japan Society for the Promotion of Science (JSPS), Grant-in-Aid for Scientific Research, Grant Number 18560482, 2006. Financial support to the first author provided by the Asian Development Bank (ADB) is also greatly acknowledged. The authors are also grateful to Prof. M. Oda and Prof. K. Tanimoto for their invaluable comments and suggestions on the work.

Notation

The following symbols are used in this paper:

d	Particle diameter
H	Shear cell height
N_{cell}	Total number of particles introduced into the shearing cell
$P(v_\theta)$, $P(v_r)$	Probability density of particle velocity in streaming and transverse directions
T	Granular temperature
V_w	Inner wall velocity of shear cell apparatus
V_θ, V_r	Average velocity of particles in streaming and transverse directions
u_j, v_j	Instantaneous velocity of jth particle in streaming and transverse directions

v'_θ, v'_r	Root-mean-square (RMS) fluctuation velocity in streaming and transverse directions
x_{1j}, y_{1j}	Coordinates of jth particle recorded at frame 1.
$\dot{\gamma} = V_w / H$	Shear rate
$\dot{\gamma}_{eff}$	Effective shear rate
θ	Particle collision angle between two particles
ν	Two-dimensional average solid fraction
ν^*	Two-dimensional normalized solid fraction
ν_m	Maximum packing factor for disks
ψ	Direction angle of particle trajectory

References

Alam, M., Luding, S. (2003) "First stress difference and crystallization in a dense sheared granular fluid." *Physics of Fluids*, 15(8), 2298–2312.

Bagnold, R. A. (1954) "Experiments on a gravity-free dispersion of large solid spheres in a Newtonian fluid under shear." *Proc. R. Soc. London*, A 225, 49–63.

Bocquet, L., Losert, W., Schalk, D., Lubensky, T.C., Gollub, J.P. (2002) "Granular shear flow dynamics and forces: Experiment and continuum theory." *Physical Review E*, 65(1), 011307.

Campbell C. S. (1990) "Rapid Granular Flows." *Annu. Rev. Fluid Mech*., 22, 57–92.

Drake, T.G. (1991) "Granular flow: physical experiment and their implications for microstructural theories." *Journal of Fluid Mechanics*, 225, 121–152.

Elliot, K.E., Ahmadi, G., Kvasnak, W. (1998) "Couette flows of a granular monolayer – an experimental study." *Journal of Non-Newtonian Fluid mechanics*, 74(1–3), 89–111.

Haff, P. K. (1986) "A physical picture of kinetic granular fluids." *J. Rheology*, 30(5), 931–948.

Hanes, D.M., Inman, D.L. (1985) "Observations of rapidly flowing granular fluid flow." *Journal of Fluid Mechanics*, 150, 357–380.

Hsiau, S.S., Jang, H.W. (1998) "Measurements of velocity fluctuations of granular materials in a shear cell." *Experimental Thermal and Fluid Science*, 17(3), 202–209.

Hsiau, S.S., Shieh, Y.H. (1999) “Fluctuations and self-diffusion of sheared granular material flows.” *Journal of Rheology*, 43(5), 1049–1066.

Hsiau, S.S., Wang, P.C., Tai, C.H. (2002) “Convection cells and segregation in a vibrated granular bed.” *A.I.Ch.E Journal*, 48(7), 1430–1438.

Hsiau, S-S, Yang, W-L (2005) “Transport property measurements in sheared granular flows.” *Chemical Engineering Science*, 60(1), 187–199.

Hunt, M. L., Zenit, R., Campbell, C. S., Brennen, C. E. (2002) “Revisiting the 1954 suspension experiments of R. A. Bagnold.” *J. Fluid Mech*., 452, 1–24.

Iwashita, K., Ichiba, K.; Oda, M. (2004) “Observations of rapidly sheared granular materials.” *J. JSCE*, 764/III-67, 147–156.

Jenkins, J.T., Richman, M.W. (1985) “Kinetic theory for plane flows of a dense gas of identical, rough, inelastic, circular disks.” *Physics of Fluids*, 28(12), 3485–3494.

Jenkins, J.T., Savage, S.B. (1983) “A theory for rapid flow of identical, smooth, nearly elastic spherical particles.” *Journal of Fluid Mechanics*, 130, 187–202.

Johnson, P.C. Jackson, R. (1987) “Frictional-collisional constitutive relations for granular materials, with application to plane shearing.” *Journal of Fluid Mechanics*, 176, 67–93.

Lun, C.K.K., Savage, S.B., Jeffrey, D.J., Chepurnity, N. (1984) “Kinetic theories for granular flow: inelastic particles in Couette Flow and slightly inelastic particles in a flow field.” *Journal of Fluid Mechanics*, 140, 233–256.

MIDI, G.D.R. (2004) “On dense granular flows.” *Eur. Phys. J. E*, 14(4), 341–365.

Mueth, D. M. (2003) “Measurements of particle dynamics in slow, dense granular Couette flow.” *Physical Review E*, 67(1), 011304.

Natarajan, V.V.R., Hunt, M.L., Taylor, E.D. (1995) “Local measurements of velocity fluctuations and diffusion coefficients for a granular material flow.” *Journal of Fluid Mechanics*, 304, 1–25.

Oda, M., Iwashita, K. (eds.) (1999) “Mechanics of granular materials.” A. A. Balkema.

Ogawa, S. (1978) “Multi-temperature theory of granular materials.” *In: Proceedings of US-Japan Seminar on Continuum-Mechanical and Statistical Approaches in the Mechanics of Granular Materials, Tokyo*. 208–217.

Savage, S.B., Jeffrey, D.J. (1981) “The stress tensor in a granular flow at high shear rates.” *Journal of Fluid Mechanics*, 110, 255–272.

Savage, S.B., Sayed, M. (1984) “Stresses developed by dry cohesionless granular materials in a annular shear cell.” *Journal of Fluid Mechanics*, 142, 391–430.

Veje, C., Howell, D., Behringer, R.P. (1999) “Kinematics of a two-dimensional granular Couette experiment at the transition to shearing.” *Physical Review E*, 59(1), 739–745.

Wang, D.G., Campbell, C.S. (1992) “Reynolds analogy for a shearing granular materials.” *Journal of Fluid Mechanics*, 244, 527–546.

Warr, S., Jacques, G.T.H., Huntley, J.M. (1994) “Tracking the translational and rotational motion of granular particles: use of high-speed photography and image processing.” *Powder Technology*, 81(1), 41–56.

Table 1. Capacity of experimental apparatus.

Parameter	Value
Motor speed	3~180 *rpm*
Shear range, $\dot{\gamma}$	5~120 sec^{-1}
Maximum torque of motor	15 *N-m*
Radius of inner wall	28.5 *cm*
Radius of outer wall	40 *cm*
Diameter of flange	2.47 *cm*
No. of flanges attached to inner wall	37 No.
No. of flanges attached to outer wall	52 No.

Table 2. Physical properties of disk used in the experiment.

Parameter	Value
Diameter, D (mm)	23
Thickness (mm)	6
Weight (g)	2.306
Density (g/cm^3)	0.934
Maximum packing factor, ν_{2DM}	0.795
Coefficient of restitution, e	0.870
Coefficient of friction, μ	0.265

Table 3. Capacity of high-speed video camera.

Parameter	Value
Frame rate	3~1,000 *Hz*
Shutter speed	30~10,000 *Hz*
Number of pixels	1,280x640
Number of frames possible	4,096
Type of color	Monochrome

Table 4. Detail of shear rate and solid fraction.

Solid fraction, ν	Normalized fraction, ν^*	Particle used in shear cell	Shear rate sec^{-1}
0.478	0.60	260	25.0~37.1
0.557	0.70	303	17.8~37.1
0.597	0.75	325	15.4~34.7
0.636	0.80	346	10.6~25.0

List of Figures

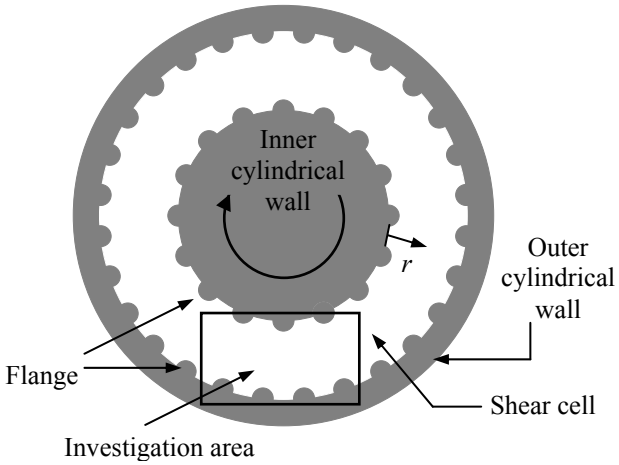

(a) Plan view of shear cell

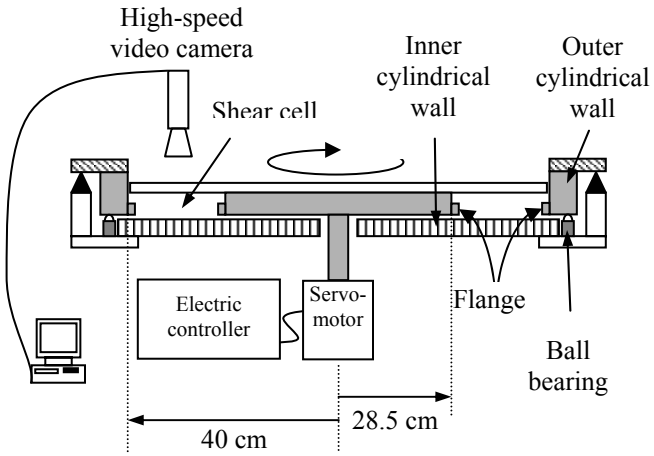

(b) Cross section of shear cell

Fig. 1. Sketch of shear cell showing (a) plan view, and (b) cross section.

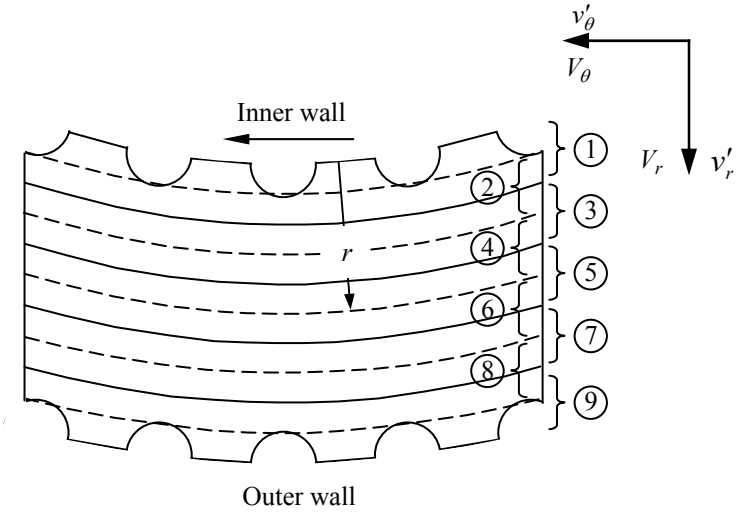

Fig. 2. Schematic of overlapping bins in the investigation area for average and fluctuating velocity measurement.

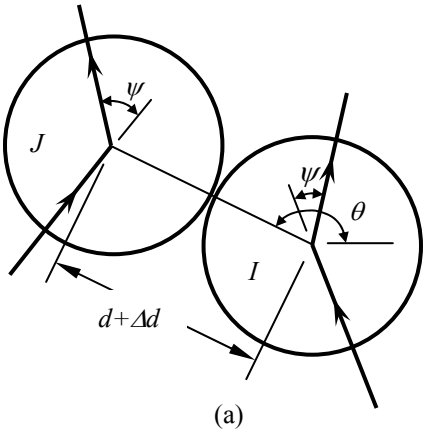

(a)

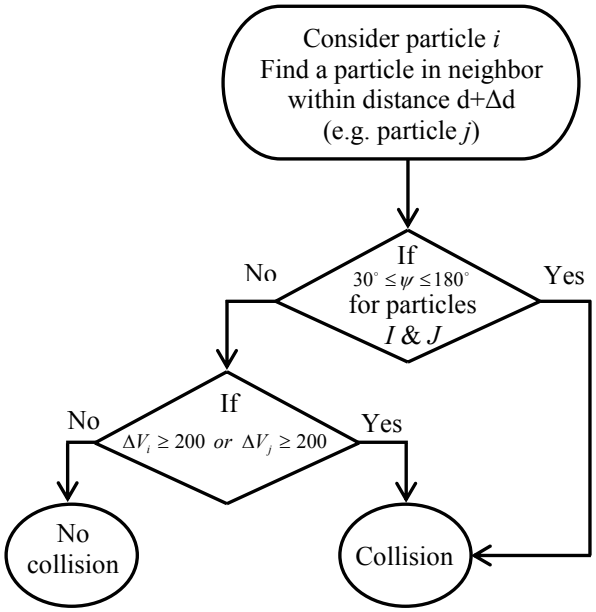

(b)

Fig. 3. (a) Definition of collision angle θ, direction angle ψ and (b) interparticle collision algorithm.

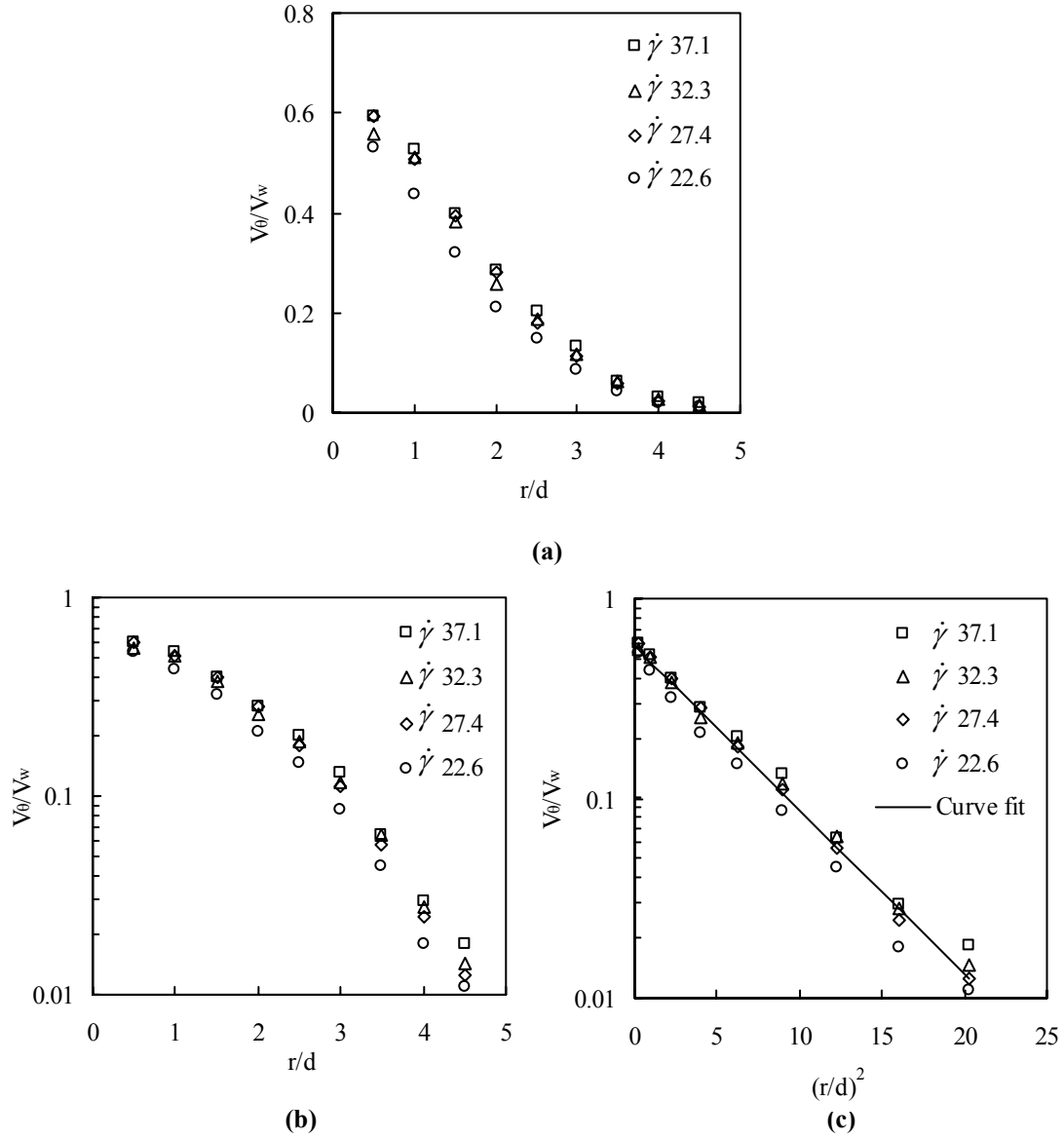

Fig. 4. Average velocity profile in streaming direction for normalized fraction of 0.70. (a) Dimensionless velocity V_θ/V_w as the function of r/d. (b) Same profile: Log (V_θ/V_w) as function of r/d. (c) Same profile: Log (V_θ/V_w) as function of $(r/d)^2$.

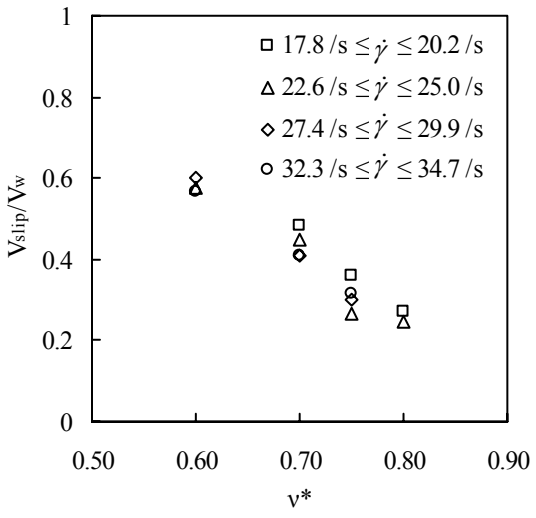

(a)

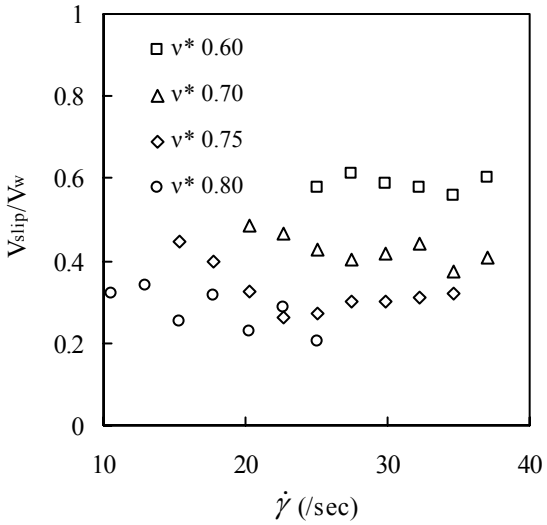

(b)

Fig. 5. Variation of slip velocity with (a) normalized fraction, and (b) shear rate.

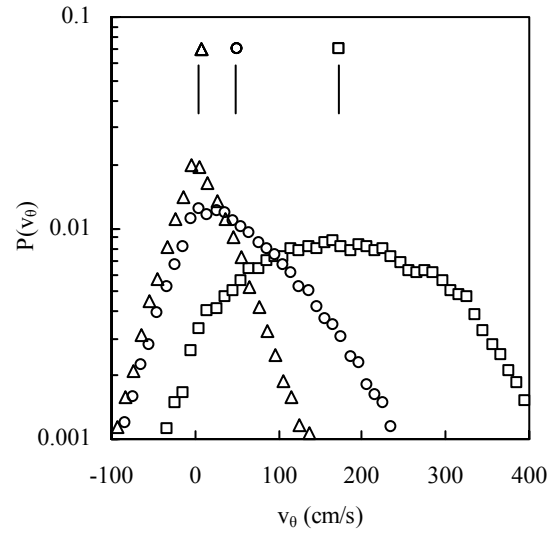

(a)

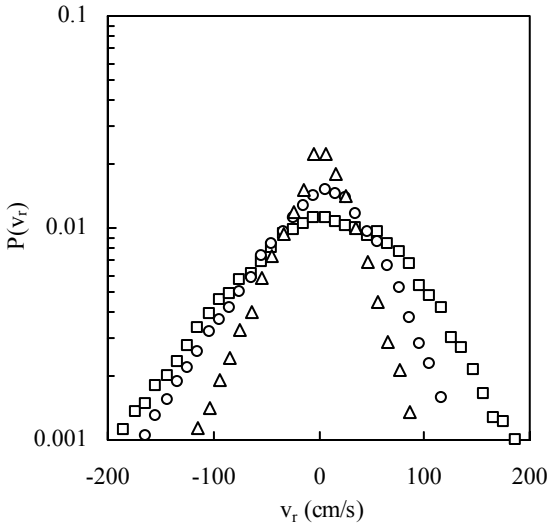

(b)

Fig. 6. Distribution of particle velocity components for normalized fraction of 0.80 and shearing rate of 25 sec^{-1} in (a) streaming and (b) transverse direction.

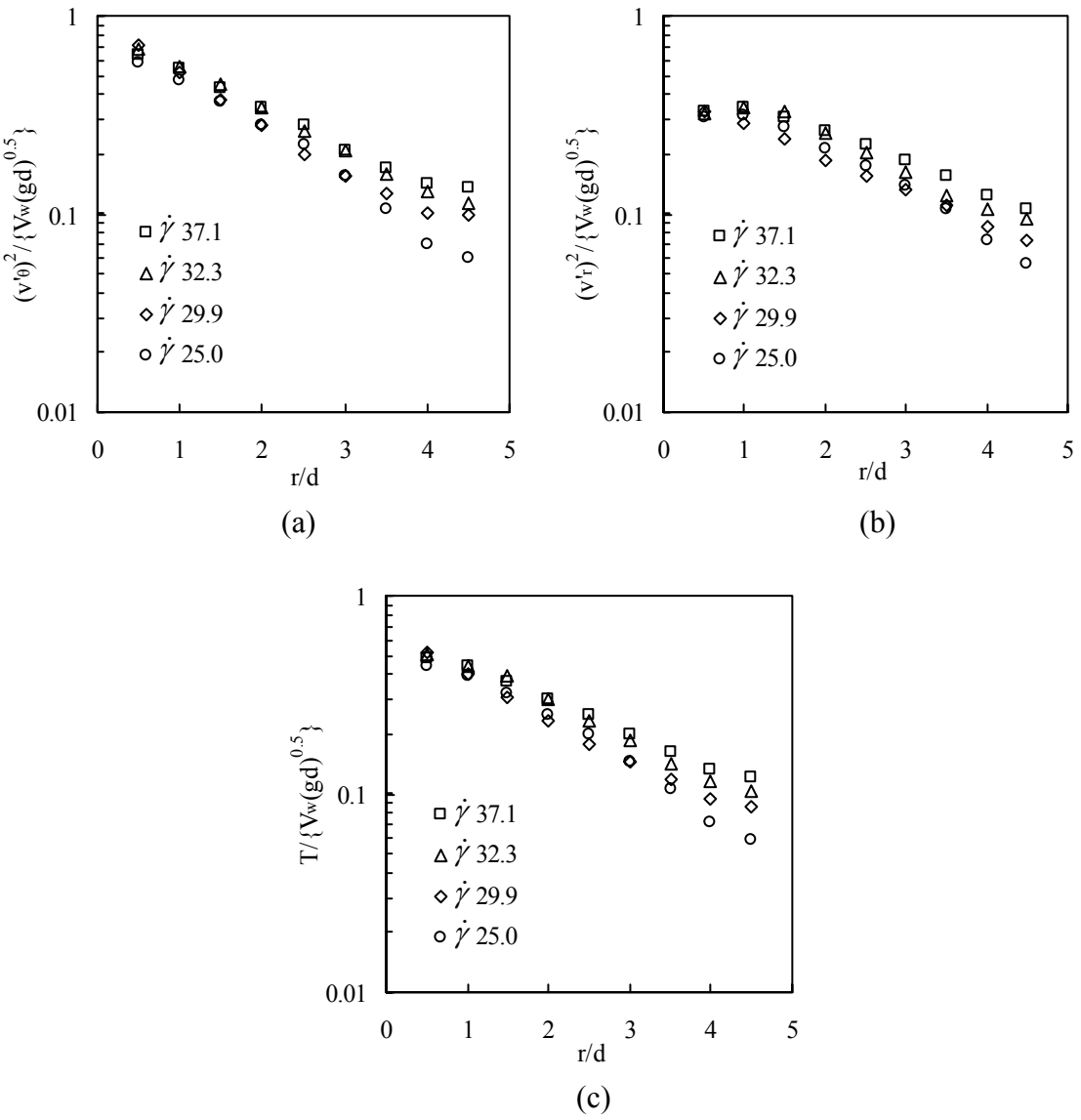

Fig. 7. Velocity fluctuation and granular temperature profile on log-linear plot for normalized fraction of 0.60. Velocity fluctuations in (a) streaming direction, (b) transverse direction and (c) granular temperature are normalized with shear rate and plotted as function of *r/d*.

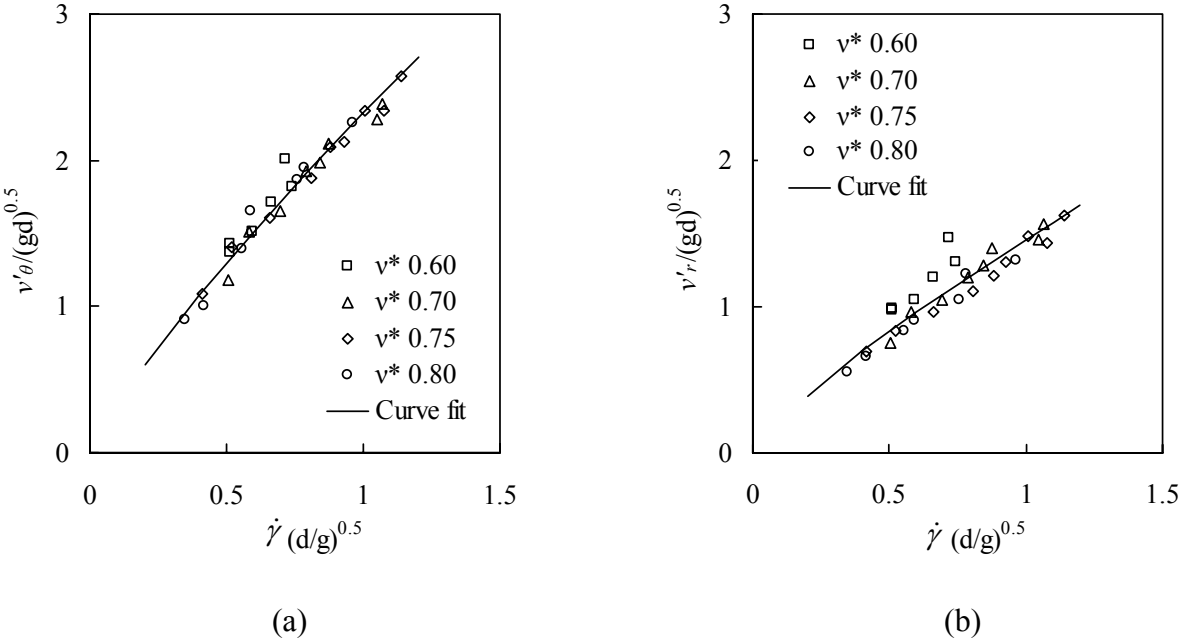

Fig. 8. Relationship between fluctuation velocity components and effective shear rate in (a) streaming direction and (b) transverse direction.

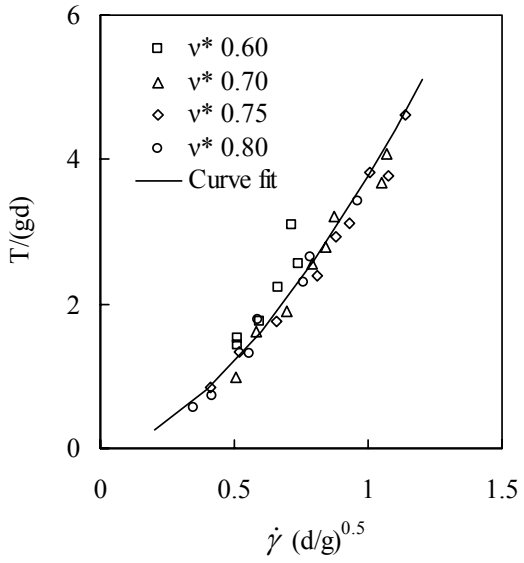

Fig. 9. Relationship between granular temperature and effective shear rate. The data is well fitted by power-law (solid line) with slope of α = 1.65.

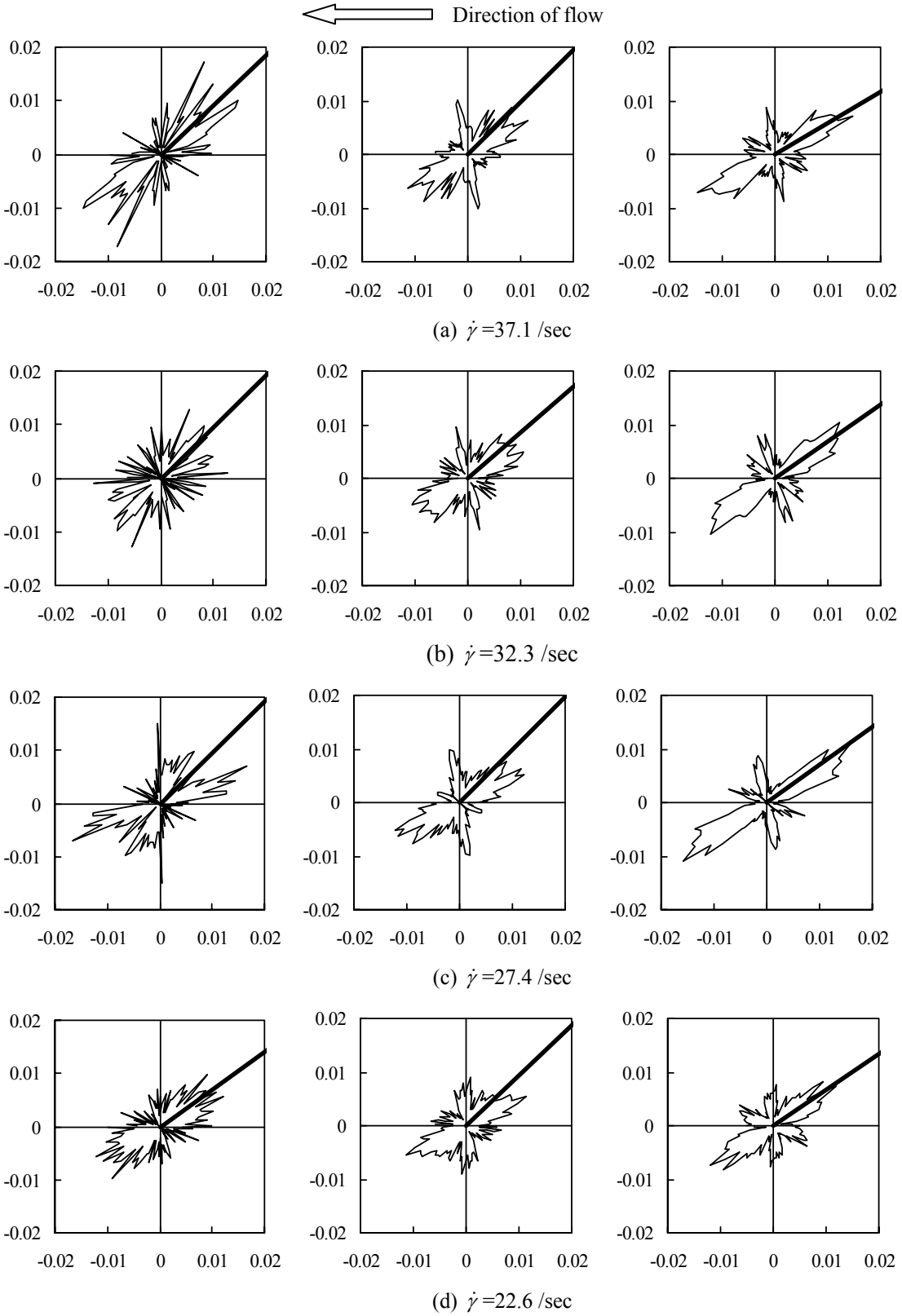

Fig. 10. Probability distribution of collision angles for solid fraction of 0.70. The graph on left is for $0 < r/d < 2$, in middle for $1.5 < r/d < 3.5$, and on right for $3 < r/d < 5$. The bold solid line shows the direction of principal angle determined through fabric tensor analysis.

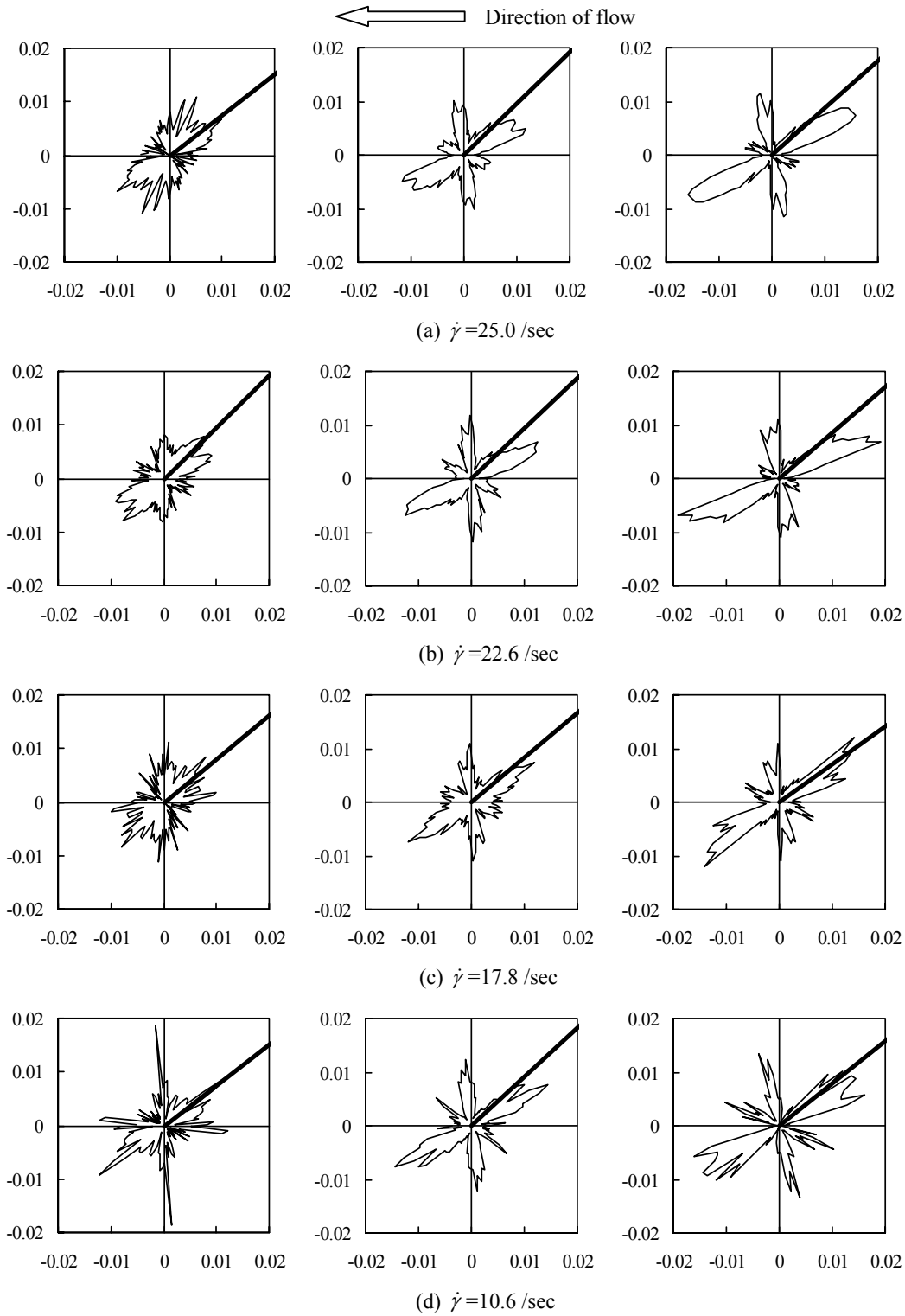

Fig. 11. Probability distribution of collision angles for solid fraction of 0.80. The graph on left is for $0 < r/d < 2$, in middle for $1.5 < r/d < 3.5$, and on right for $3 < r/d < 5$. The bold solid line shows the direction of principal angle determined through fabric tensor analysis.

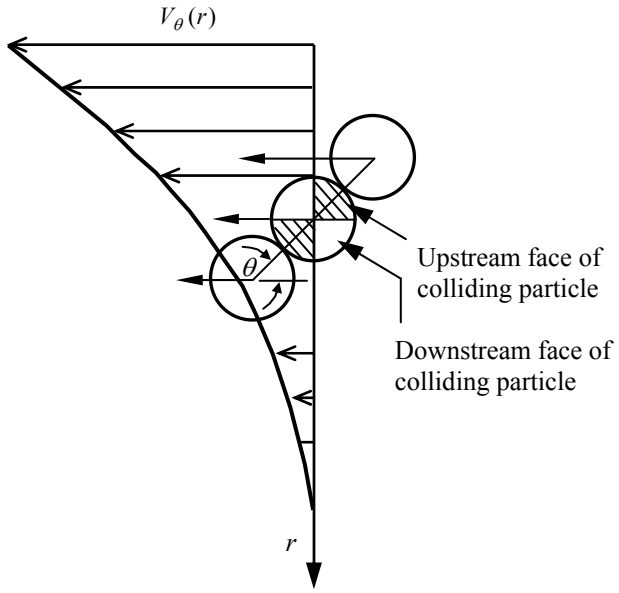

Fig. 12. The schematic of the possible collision angles θ in uniform shear flow; θ is measured anticlockwise from the positive x-axis.